Live Load Distribution Factors for a Lightweight Movable Bridge Deck System

Hadi Baghi

Louisiana Tech University, Ruston, LA, USA

Fatmir Menkulasi

Wayne State University, Detroit, MI, USA

Jacob Parker

SDR Engineering Consultants, Baton Rouge, LA, USA

Contact: hadibaghi@gmail.com

Abstract

Louisiana has approximately 160 movable bridges, mostly in the southern part of the state. The typical deck systems in these movable bridges are steel grids. Records show that steel grids have had maintenance issues. A precast lightweight concrete deck system for Louisiana's movable bridges is presented. The deck configuration features a multi-rib T-beam configuration. Live load distribution factors (LLDFs) for flexure and shear are quantified so that the deck system can be designed using the traditional beam line analysis method. Several nonlinear finite element analyses were conducted to quantify worst case LLDFs for interior and exterior ribs. A variety of load positions and span configurations are examined. LLDFs for moment and shear vary from 0.63 to 0.87, and from 0.64 to 0.86, respectively. The LLDFs for flexure and shear provided in this paper offer a practical approach for designing this new deck system for movable bridges.

Keywords: Movable bridge decks; live load distribution factors; finite element analysis

1 Introduction

Louisiana has approximately 160 movable bridges, mostly in the southern part of the state. This places Louisiana among the states with the highest inventory of movable bridges in the nation. The typical deck systems in movable bridges are open steel grids, which typically consist of either diagonal or rectangular grids (Fig. 1). The traditional steel grid decks are supported by steel stringers at typically 1.22 m on center. On average these decks weigh less than 1.20 kN/m^2; while some others can weigh as little as 0.67 kN/m^2 [1]. This deck system is attractive because it is light weight, the panels are prefabricated and they are easy to install and replace. However, records show that steel grids have exhibited durability issues. The proximity of these exposed steel systems to humid environments leads to rapid deterioration. As a result, decks become loose, causing extreme noise. These problems are aggravated by trapping foreign debris throughout the deck grids. Other problems associated with steel grid decks are unpleasant ride quality caused by panels becoming loose, and possible safety issues caused by a reduction in skid resistance due to use and deterioration.

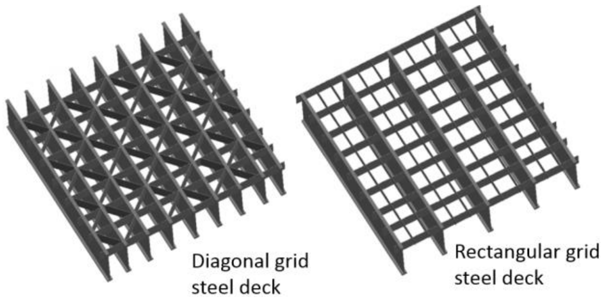

Figure 1. Steel grid decks for movable bridges

The Louisiana Department of Transportation and Development (LADOTD) has an interest in using concrete decks to replace deteriorated steel grids on existing movable bridges as well as in new construction. However, the mechanical systems of moveable bridges are highly sensitive. As a result, any decking used to replace or rehabilitate the existing steel grid decking should match the weight of the existing steel grid such that the mechanical system operates as designed.

Florida Department of Transportation (FDOT) in collaboration with URS Corporation identified several potential alternative lightweight solid deck systems to replace steel open grid decks on typical Florida bascule bridges [1], [2]. The concrete deck systems featured the proprietary concrete mix *Ductal* marketed by Lafarge.

Baghi et al. [3] developed a modified version of the waffle slab developed in Florida using *Ductal* to comply with maximum weight, span length and overall depth requirements established for Louisiana's movable bridges. These requirements were as follows: 1) the maximum span considered was 1270 mm; 2) the overall depth of the deck was 132 mm to comply with existing steel grid deck thicknesses; 3) the maximum weight of the panel was 0.96 kN/m^2.

Menkulasi et al. [4] developed four high performance concrete deck panel configurations for Louisiana's movable bridges using four distinct non-proprietary concrete mixes. All deck configurations featured either a waffle slab or a T-beam geometry (i.e. they either featured transverse and longitudinal ribs or just transverse ribs). The deck configuration that used the LWHPC130 mix featured the simplest geometry and was selected for future investigations. This deck configuration features only transverse ribs. LWHPC stands for lighter weight high performance concrete and the number 130 was used to distinguish it from the other investigated lighter weight mixes. The mix design as well as the material properties for LWHPC130 are provided in Tables 1 and 2.

The most unique feature of the LWHPC130 mix was the introduction of expanded quartz Poraver beads manufactured by Poraver. The expanded quartz Poraver beads were introduced to reduce the unit weight of the mix by replacing a portion of the fine sand. Poraver beads are lightweight aggregates manufactured from post-consumer recycled glass, which is available in a variety of sizes. Some of their key advantages are their low density and high strength

All the concrete deck configurations developed by Baghi et al. [3] and Menkulasi et al. [4] were based on nonlinear finite element analyses. The goal of the research presented in this paper is to develop live load distribution factors for the deck configuration that features the LWHPC130 mix so that each transverse rib can be designed as a T-beam. This will open the way for establishing a design framework for the newly developed concrete deck systems for movable bridges that is suitable for a design office.

Table 1. Mix design for four high performance concrete mixes

Ingredients	LWHPC130 [kg/m^3]
Portland cement I/II[a]	712
Silica Fume[b]	231
Fly Ash	0
Glass powder[b]	211
Fine Sand[c]	449
Poraver Beads[d]	199
6.35 mm max. coarse aggregate	0
Water	183
HRWR	52
Steel Fibers[e]	156
W/Cm	0.19

[a]Supplied by Ash Grove, [b]Supplied by Quadex, Inc., [c]Silica sand supplied by US Silica, [d]Supplied by Poraver, [e]Produced my Dramix.

Table 2. Materials properties for LWHPC130

Material Property	Value
Unit weight, γ [kg/m^3]	122
Compressive strength, f'_c [MPa]	73
Tensile strength [MPa]	
a) first crack [f_{tm}]	6.2
b) peak strength [f_{tu}]	14.3
Modulus of elasticity (E) [MPa]	28000
Poisson's ratio (υ)	0.17

2 Deck Panel Description

Figure 2 shows the top view of the concrete deck system with the LWHPC130 mix and features two adjacent precast deck panels in the transverse direction of the bridge (perpendicular to traffic). The gray bands represent the cast-in-place concrete continuity diaphragm and cast-in-place concrete fill between adjacent precast deck panels. Figure 3 shows the details of the deck panel configuration, which features only transverse ribs and offers a simple geometry. All reinforcing bars are GFRP V-ROD HM – 60 GPa Grade III. These GFRP bars are corrosion resistant and are manufactured by Pultrall Inc. The thickness of the flange is 32 mm. Top flange reinforcing consists of No.10 GFRP bars at 76 mm on center in the longitudinal direction and 152 mm on center in the transverse direction. The width of the stem in the transverse ribs is 51 mm to accommodate the No. 19 GFRP bar (Detail A). The exterior ribs are reinforced with No.19 bars at the bottom and have a width of 44 mm (Detail B). Continuity in the direction of traffic is provided by using female-to-female type panel to panel connections and a cast-in-place HPC fill (Detail B). The good bond characteristics between the precast and cast-in-place HPC mixes are expected to emulate monolithic action.

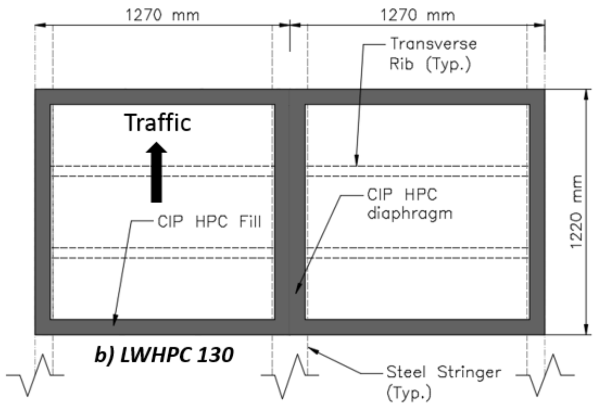

Figure 2. Top view of the concrete deck system

At the ends of the precast panels in the transverse direction there is a 48 mm wide cast-in-place continuity diaphragm (Detail C). This diaphragm helps provide continuity in the transverse direction. Headed studs welded on the top flange of steel stringers help create composite action, which enhances the stiffness of deck system compared to the steel grids where such composite action could not be relied upon. The top flange at the edges of each panel is coped 76 mm in length and 16 mm in depth to allow the GFRP bars to project past the ends of the panels, be immediately above the coped flange and lap with the GFRP bars from the adjacent panel (Detail B and C). The GFRP bars project 76 mm past the edges of the panel to create a 152 mm lap with the bars coming from the adjacent panel. The self-weight of the deck panel considering the site cast concrete is 0.95 kN/m^2.

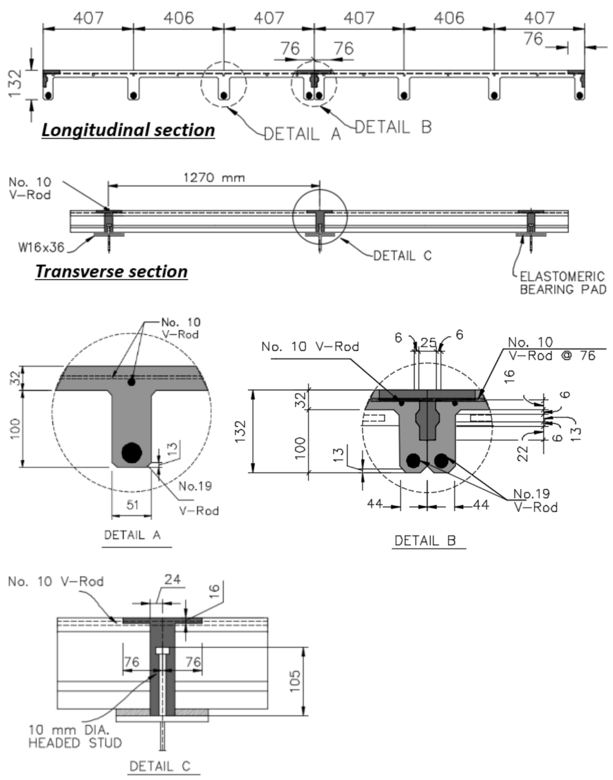

Figure 3. Details of the concrete deck system (all dimensions are in mm)

3 Finite Element Analyses

Several nonlinear finite element analyses were conducted to compute live load distribution factors for moment and shear in each transverse rib. The service level load based on AASHTO LFRD Specifications [5] was used in each case to compute LLDFs. Service level load (95 kN) was calculated as the load corresponding to one wheel for an HL-93 truck (71 kN) times the dynamic load allowance (1.33).

Because the panels were expected to exhibit cracking under service level loading, nonlinear finite element analyses were conducted to capture the effects of cracking and material nonlinearity. The nonlinear behavior of concrete was simulated using the concrete damage plasticity approach available in Abaqus [6] developed by Lubliner et al. [7] and Lee and Fenves [8]. The uniaxial behavior of concrete in compression and tension was based on material characterization tests conducted by Menkulasi et al. [4] and is illustrated in Figure 4. Table 3 provides values for compressive strength, tensile strength, modulus, Poisson's ratio, and unit weight. The stress-strain relationship for the GFRP bars is linear elastic and was based on data provided by the manufacturer. The modulus of elasticity for the GFRP bars varies from 63 GPa to 66 GPa and the ultimate stress varies from 1000 MPa to 1370 MPa. The bond between GFRP bars and concrete was assumed to be perfect. To validate this assumption the computed maximum stress on the rebars computed from finite element analysis was compared with the developable stress calculated using the guidelines provided in ACI 440.1 [9].

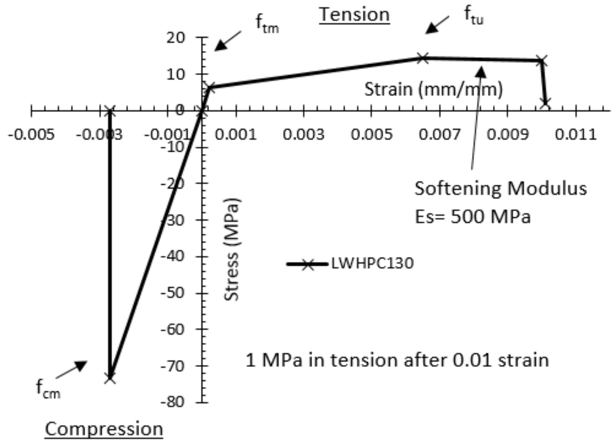

Figure 4. Uniaxial behavior of concrete in compression and tension

Table 3. Material properties for LWHPC130 mix

Material property	Value
Compressive strength	f'_c = 10.7 MPa
Tensile strength, first crack (f_{tm}), ultimate stress (f_{tu})	f_{tm} = 0.9 MPa f_{tu} = 2.08 MPa
Modulus of elasticity	E = 28000 MPa
Poisson's ratio	υ= 0.17
Unit weight	γ = 1954 kg/m^3

Two deck panel configurations were considered for computing live load distribution factors: 1) a single span configuration; and 2) a two span continuous configuration. Figure 5 illustrates the wheel load positions used to compute LLDFs for moment. In the single span configuration only one wheel load could be accommodated on the deck panel because the spacing between the wheels is 1829 mm whereas the distance between the centerlines of the stringers is 1270 mm. In the two span continuous configuration one full wheel load and a portion of the second wheel load pertaining to the same axle could be accommodated. In the single span configuration the wheel load was centered at mid-span to maximize bending moment. In the two span continuous configuration the wheel load was centered at the mid-span of one of the spans.

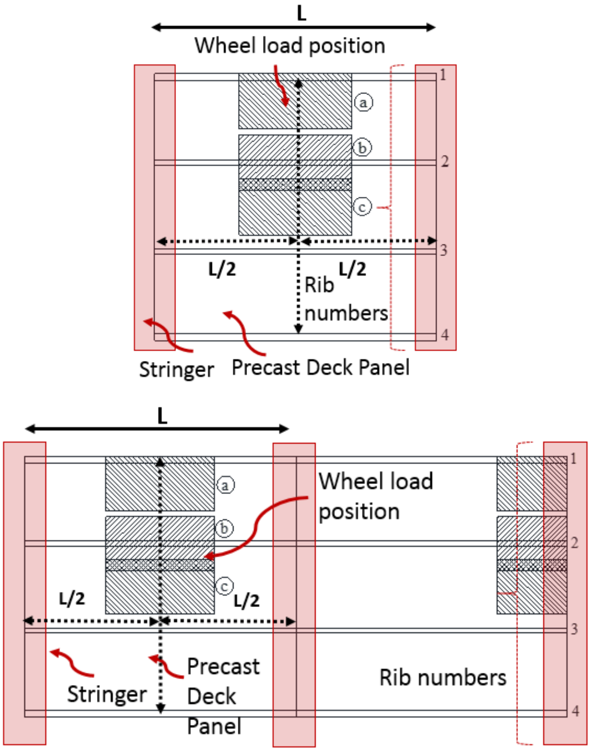

Figure 5. Wheel load positions for determining LLDFs for moment

A total of three wheel load positions were considered for each case namely *a*, *b*, and *c.* Figure 6 shows the deformed configuration of the deck for each one of these wheel load positions. Vertical deflection contours are also shown to illustrate the deformation of each rib. Load position *a* represents a case when the edge of the wheel load patch aligns with the edge of a precast deck panel. This load position is intended to maximize load effects on the exterior rib. Load position *b* represents a case when the center of the wheel load is aligned with the center of one of the interior ribs. This load position is intended to maximize load effects on the interior ribs. Finally, load position *c* represents a case when the center of the wheel load is aligned with the mid-width of the precast panel.

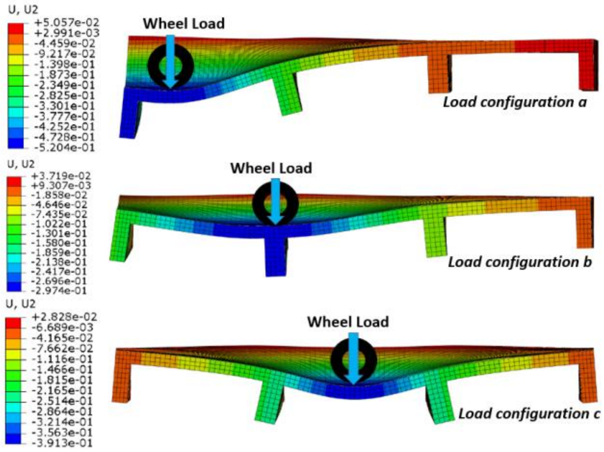

Figure 6. Deformed configuration of the deck under each load position (vertical deflection in inches, 1 in. = 25.4 mm).

Live load distribution factors (LLDFs) for moment in an individual rib were calculated using Equation 1, in which the curvature in an individual rib was divided by the sum of curvatures in all ribs. The curvature was calculated based on the strain diagram obtained for each rib at mid-span and was calculated by summing the top and bottom strain at the most extreme fibers and by dividing them with the depth of the deck (Figure 7 and Equation 2).

$$LLDF(M)_i = \frac{\varphi_i}{\sum_{i=1}^{n} \varphi_i} \qquad (1)$$

where

$\mathrm{LLDF(M)_i}$ = live load distribution factor for moment in an individual rib
φ_i= curvature in an individual rib
n = number of ribs

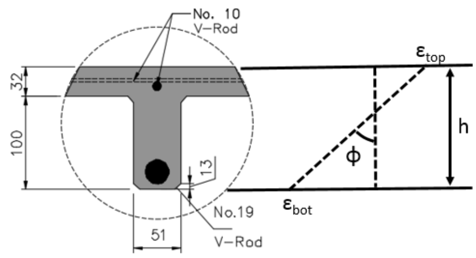

Figure 7. Calculation of curvature in each rib (all dimensions are in mm)

$$\varphi = \frac{(\varepsilon_{top}+\varepsilon_{bot})}{h} \qquad (2)$$

where

ε_{top}= strain in the top fiber
ε_{bot}= strain in the bottom fiber
h = deck depth

Figure 8 shows the strain diagrams in interior and exterior ribs for load position *c*. Both strain diagrams suggest that plane sections remain plane under service load conditions. The maximum tensile strain exceeds the first cracking strain of 0.00003 in both cases.

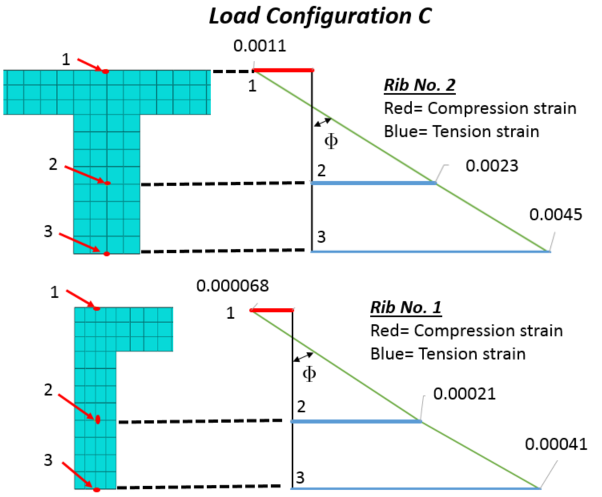

Figure 8. Strain diagram and curvature in interior and exterior ribs

Figure 9 shows the wheel load positions investigated for computing LLDFs for shear. The edge of the wheel patch was placed at a distance *d* from the face of support to maximize shear effects at the critical section for shear (where *d* is the effective depth of the deck section). In the single span configuration only one wheel load could be accommodated, whereas in the two span continuous configuration two full wheel loads could be accommodated. Live load distribution factors for shear were calculated using Equation 3, where the reaction in each rib was divided by the sum of reactions in all ribs.

$$LLDF(V)_i = \frac{R_i}{\sum_{i=1}^{n} R_i} \qquad (3)$$

where

$\mathrm{LLDF(V)_i}$ = live load distribution factor for shear in an individual rib
$\mathrm{R_i}$= reaction in an individual rib
n = number of ribs

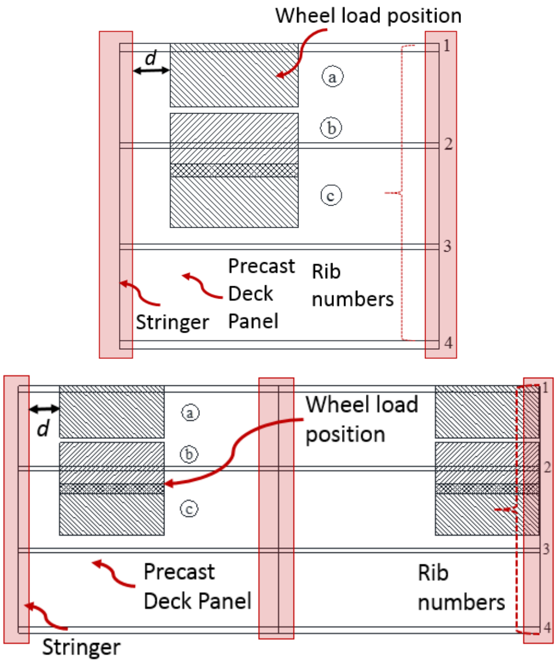

Figure 9. Wheel load positions for determining LLDFs for shear

4 Live Load Distribution Factors

Figure 10 illustrates the LLDFs for moment for the single span and two span continuous configuration. For the two span continuous configuration distribution factors were calculated for both positive and negative moments. There is not a clear trend as to which configuration resulted in the highest distribution factors for moment. For example, for load position *a*, the maximum distribution factor for positive moment was calculated for the single span configuration, although the difference with the two span continuous configuration was small (0.63 versus 0.57). For load positions *b* and *c*, the two span continuous configuration resulted in higher distribution factors for positive moment, although the difference for load position *c* was very small (0.46 versus 0.48). The maximum distribution factor for positive moment for interior and exterior ribs was 0.68 and 0.63, respectively.

Figure 11 illustrates the distribution factors for negative moment for the two span continuous configuration. The distribution factors are higher than those calculated for positive moment. For example the maximum distribution factors for negative moment for exterior and interior ribs are

0.74 and 0.87, respectively, as opposed to 0.63 and 0.68 for positive moment.

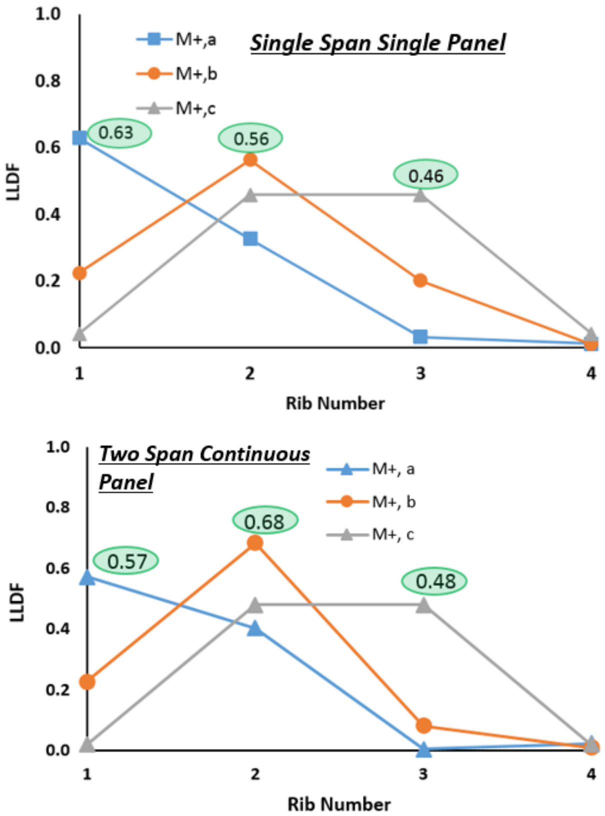

Figure 10. LLDF (+M)

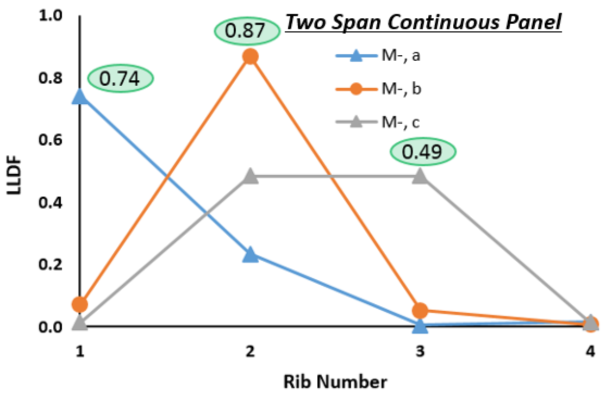

Figure 11. LLDF (-M)

Figure 12 illustrates live load distribution factors for shear for the single span and two span continuous configuration. The two span continuous configuration resulted in higher distribution factors for shear for all investigated load positions. The highest distribution factor for shear in interior and exterior ribs are 0.86 and 0.64, respectively.

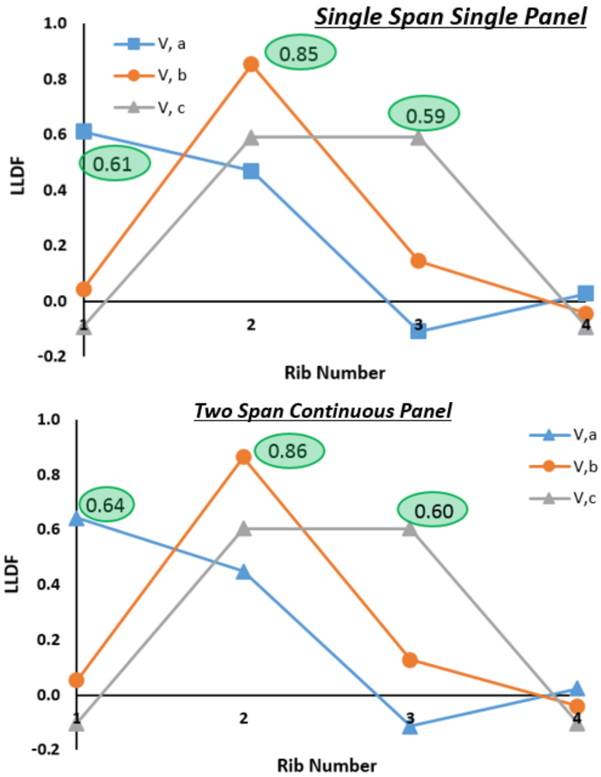

Figure 12. LLDF (V)

5 Design Framework

The live load distribution factors for moment and shear determined in the previous section can be used to design the newly developed deck for movable bridges using beam line analysis. A sectional analysis approach can be adopted to design the interior and exterior ribs for flexure and shear. Flexural resistance can be based on conditions of equilibrium of forces and strain compatibility. Recommendations by Graybeal [10] can be used as a starting point to quantify the flexural strength. For shear, the recommendations of Baby et al. [11] can be used to evaluate the shear strength of the T-shaped cross-sections. However, all strength prediction models need to be validated based on physical tests or nonlinear finite element analyses. Such a task was outside the scope of this paper and is currently being conducted by the authors.

6 Conclusions

A precast lightweight deck system for Louisiana's movable bridges was presented. The deck configuration features a multi-rib T-beam configuration and was selected because of its ease of fabrication. Live load distribution factors (LLDFs) for flexure and shear were quantified so that the deck system can be designed using the traditional beam line analysis method. Several nonlinear finite element analyses were conducted to quantify worst case LLDFs for interior and exterior ribs. A variety of load positions and span configurations were examined. The span configurations featured simply supported and continuous configurations.

The worst case LLDFs for positive moments in the interior and exterior ribs are 0.68 and 0.63, respectively. The worst case LLDFs for negative moments in the interior and exterior ribs are 0.87 and 0.74, respectively. For shear, the highest LLDFs are 0.86 for an interior rib and 0.64 for an exterior rib. The LLDFs for flexure and shear provided in this paper offer a practical approach for designing this new deck system for movable bridges.

A design approach based on beam line analysis was presented for the newly developed concrete deck system. The live load distribution factors presented in this paper will be combined with the results from nonlinear finite element analyses provided by Menkulasi et al. [4] as well as those obtained from physical tests scheduled in the near future to prepare a design guide that can be used by state DOTs and consulting firms.

7 Acknowledgements

This study was sponsored by the Louisiana Transportation Research Center (LTRC) and Louisiana Department of Transportation and Development (LADOTD). The authors would like to thank the project review committee for their comments and their thorough review of the work performed to date. The authors would also like to thank Quadex, Inc. for donating the silica fume and glass powder. The opinions expressed herein are those of the authors and do not necessarily reflect the views of the sponsor.

8 References

[1] Mirmiran, A., Saleem, M., A., Mackie, K., Xia, J. Alternatives to steel grid decks, Draft Final Report, Florida Department of Transportation Research Center, FDOT Contract No. BD015RPWO#22, 2009, Tallahassee, FL.

[2] Mirmiran, A., Ghasemi, S. Lightweight Solid Decks for Movable Bridges – Phase II, Final Report, Florida Department of Transportation Research Center, FDOT Contract No. BDV29-977-11, 2016, Tallahassee, FL.

[3] Baghi, H., Menkulasi, F., Parker, J., Barros, J.O.A. Development of a High Performance Concrete Deck for Louisiana’s Movable Bridges: Numerical Study, Journal of Bridge Engineering, Accepted, 2017.

[4] Menkulasi, F., Montes, C., Baghi, H., Parker, J. Development of a Sustainable UHPC Bridge Deck for Movable Bridges, Interim Report 2, May 2016, Louisiana Transportation Research Center, Baton Rouge, LA.

[5] AASHTO LRFD Bridge Design Specifications (2013), 6th Edition, Washington, DC.

[6] Abaqus [Computer Software]. Dassault Systèmes Americas Corp., Waltham, MA.

[7] Lubliner, J., Oliver, J., Oller, S., Oñate, E. A Plastic-Damage Model for Concrete, International Journal of Solids and Structures, 1989, 25 (3), 229–326.

[8] Lee, J., Fenves, G. L. Plastic-Damage Model for Cyclic Loading of Concrete Structures, Journal of Engineering Mechanics, 1998, 124 (8), 892–900.

[9] ACI 440.1R-06. Guide for the Design and Construction of Structural Concrete Reinforced with FRP Bars, American Concrete Institute, 2006, Farmington Hills, MI.

[10] Russell, H. G., Graybeal, B. A. Ultra-high performance concrete: A state-of-the-art report for the bridge community, 2013, Federal Highway Administration, Washington DC.

[11] Baby, F., Billo, J., Renaud, J.C., Massotte, C., Marchand, P., Toutlemonde, F., Simon, A., Lussou, P. Shear Resistance of Ultra High Performance Fibre Reinforced Concrete I-Beams, Proceedings of the 7th International Conference on Fracture Mechanics of Concrete and Concrete Structures, Jeju, Korea, May 2010, pp. 1,411–1,417.